

# On-sky silicon photomultiplier detector performance measurements for millisecond to sub-microsecond optical source variability studies

Albert W. K. Lau<sup>a,\*</sup>, Mehdi Shafiee,<sup>b</sup> George F. Smoot,<sup>b,c,d,e</sup>  
Bruce Grossan<sup>b,f</sup>, Siyang Li,<sup>g</sup> and Zhanat Maksut<sup>b</sup>

<sup>a</sup>Hong Kong University of Science and Technology, Department of Physics, Kowloon, Hong Kong, China

<sup>b</sup>Nazarbayev University, Energetic Cosmos Laboratory, Nur-Sultan, Kazakhstan

<sup>c</sup>Hong Kong University of Science and Technology, Institute for Advanced Study, Kowloon, Hong Kong, China

<sup>d</sup>Lawrence Berkeley National Laboratory, Berkeley, California, United States

<sup>e</sup>Université Sorbonne Paris Cité, Laboratoire APC-PCCP, Université Paris Diderot, Paris, France

<sup>f</sup>University of California, Space Sciences Laboratory, Berkeley, California, United States

<sup>g</sup>University of California, Department of Physics, Berkeley, California, United States

**Abstract.** In our Ultra-Fast Astronomy (UFA) program, we aim to improve measurements of variability of astronomical targets on millisecond and shorter time scales. In this work, we present initial on-sky measurements of the performance of silicon photomultiplier detectors (SiPMs) for UFA. We mounted two different SiPMs at the focal plane of the 0.7-m aperture Nazarbayev University Transient Telescope at the Assy-Turgen Astrophysical Observatory, with no filter in front of the detector. The 3 mm × 3 mm SiPM single-channel detectors have a field of view of 2.2716' × 2.2716'. During the nights of October 28–29, 2019, we measured sky background, bright stars, and an artificial source with a 100-Hz flashing frequency. We compared detected SiPM counts with Gaia satellite G-band flux values to show that our SiPMs have a linear response. With our two SiPMs (models S14520-3050VS and S14160-3050HS), we measured a dark current of ∼130 and ∼85 kilo counts per second (kcps), and a sky background of ∼201 and ∼203 kcps, respectively. We measured an intrinsic crosstalk of 10.34% and 10.52% and derived a 5σ sensitivity of 13.9 and 14 Gaia G-band magnitude for 200-ms exposures, for the two detectors, respectively. For a 10-μs window, and allowing a false alarm rate of once per 100 nights, we derived a sensitivity of 22 detected photons, or six Gaia G-band magnitudes. For nanosecond timescales, our detection is limited by crosstalk to 12 detected photons, which corresponds to a fluence of ∼155 photons per square meter. © 2020 Society of Photo-Optical Instrumentation Engineers (SPIE) [DOI: [10.1117/1.JATIS.6.4.046002](https://doi.org/10.1117/1.JATIS.6.4.046002)]

**Keywords:** Ultra Fast Astronomy; silicon photomultiplier; millisecond optical variability.

Paper 20053 received May 18, 2020; accepted for publication Nov. 6, 2020; published online Nov. 27, 2020.

## 1 Introduction

In our Ultra Fast Astronomy (UFA) program, we aim to survey the sky at sub-second (ns to ms) time scales in the optical-infrared bands.<sup>1</sup> We already know of millisecond (ms) variability among the fastest-known sources of x-ray and optical variability and transients (e.g., x-ray binaries and pulsars). Fast radio bursts have ms variations in the radio frequencies; if there were accompanying emission in the optical,<sup>2</sup> it could be orders of magnitude faster. Occultation techniques with high time resolution can provide sub-milliarcsecond accuracy on direct measurement of stellar diameters.<sup>3,4</sup> Arguments have been made that optical bands are favorable for interstellar communication due to the high bandwidth, requiring short time scale sensitivity for

\*Address all correspondence to Albert W. K. Lau, [awklau@connect.ust.hk](mailto:awklau@connect.ust.hk)

optical SETI.<sup>5</sup> In addition, we point out that probing shorter time scales at improved sensitivities could be a rich source of new discoveries, as this is a poorly covered part of the sensitivity-time scale parameter space.

The search for these sub-second transient events using traditional CCD-like detectors is limited by readout noise, readout rate, and hence frame rate. For example, the HIPERCAM system, as one of the most sensitivity CCD-based fast optical camera, can provide  $\sim 1$  frame per second (fps) on full readout mode or  $\sim 1000$  fps on drift-mode.<sup>6</sup> Therefore, non-integrating photon detectors, such as photomultiplier tubes (PMTs), silicon photomultipliers (SiPMs), or more advanced superconductive photon-counting sensors<sup>7,8</sup> are better suited for exploring even shorter time scales. Recently, we began measurements on the sky using a SiPM-based testing camera on the 0.7-m aperture Nazarbayev University Transient Telescope at the Assy-Turgen Astrophysical Observatory (NUTTelA-TAO).<sup>9</sup> In this experiment, two different models of SiPM were used to measure sky background, bright stars, and an artificial ms-period source. The experiment was performed on the nights of October 28 and 29, 2019 with an ambient temperature of roughly 0°C and a radiometric sky temperature (measured with a Boltwood Cloud Sensor II) in the range of -25°C to -30°C, with a slightly cloudy sky.

In this paper, we present our experimental setup, observation log, and data processing method. In addition, we present our calculations of detection of lower limits at different time scales, along with our measurements of SiPM crosstalk, dark count, and sky background. Finally, we propose some improvements to our system for future observations.

## 2 Experimental Setup

Figure 1 shows the setup for this experiment at Assy-Turgen Astrophysical Observatory.

### 2.1 SiPMs and Readout System

#### 2.1.1 SiPMs

SiPMs are a relatively recent technology, giving photon counting from a solid-state chip. These detectors achieve single- and multiple-photon resolving power by massive parallel Geiger mode avalanche diodes (micropixels) which produce a photon gain<sup>10</sup> of  $\sim 10^6$ . A micropixel can only receive one count within the recovery time, and multiple photons detection is achieved by summing up the signals from the parallel micropixels. It is noteworthy that the micropixels, effectively summed internally, do not give spatial resolution within a single SiPM channel.<sup>11</sup>

SiPMs have a high damage threshold for bright light exposure, a much lower working voltage, and higher overall quantum efficiency compared to PMTs. Some trade-offs of SiPMs versus PMTs include higher crosstalk and dark count noise.<sup>12</sup> In SiPMs, crosstalk is said to occur when

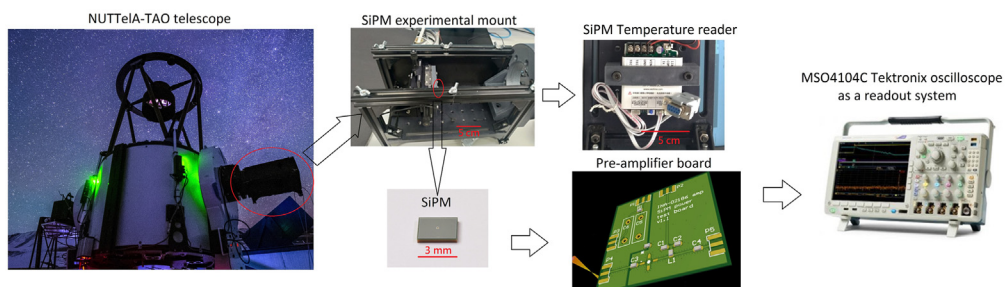


**Fig. 1** Experimental Setup. The left image shows the telescope with the SiPM experiment mounted on the instrument port at right. The four center images show the SiPM mount, hardware and electronics. The far right image shows the oscilloscope used to view the signal and acquire the data.

**Table 1** Manufacturer's specifications of the SiPMs.

Specifications testing voltage	SiPM s14160-3050HS breakdown voltage +2.70 V	SiPM s14520-3050VS breakdown voltage +3 V
Photosensitive area per channel	3 mm × 3 mm	3 mm × 3 mm
Micropixel pitch	50 μm	50 μm
Micropixels per channel	3531	3531
Spectral response range	Appendix A Fig. 13	Appendix A Fig. 14
Peak photon detection efficiency	50% at 450 nm	49% at 450 nm
breakdown voltage	38 V	38 V
Temperature coefficient of breakdown voltage	34 mV/C°	34 mV/C°
Standard overvoltage	2.70 V	3 V
Crosstalk	7%	5%
Dark count	1 Mcps	600 kcps
Photon gain	$2.5 \times 10^6$	$2.8 \times 10^6$
Optical window	Silicone, 150 μm	Silicone, 150 μm
Windows refractive index	1.57	1.57

one incoming photon triggers more than one micropixels; this occurs when nearby micropixels also contribute electrons due to electron leakage or re-emission in the semi-conductor. These are measured and discussed further in Secs. 4.4 and 5.

SiPMs' immunity to magnetic field and bright-light damage provide easiness on mechanical and experimental design. In terms of signal integrity, SiPMs are also providing better signal amplitude linearity and time-resolution compare to PMTs.<sup>11</sup> As a more recent technology, the parameters of SiPM are still in rapid improvement. SiPM-based Astronomy detectors such as the next generation of imaging atmospheric Cherenkov telescopes are emerging.<sup>11–13</sup> Therefore, we designed our fast astronomical detectors based on SiPM technology.

In this experiment, we used single-channel SiPM models S14160-3050HS and S14520-3050VS from Hamamatsu.<sup>14</sup> The manufacturer's specifications of these two models are given in Table 1 (at standard conditions at 25°C, and standard overvoltage).

The dark count noise of SiPMs is significantly reduced at a lower temperature. During the experiment, the SiPMs ran at ~0°C without any external cooling. Since the breakdown voltage of a SiPM also decreases with decreasing temperature, we carried out a breakdown voltage versus temperature measurement before the experiment at the observatory (Appendix B). The SiPM voltage was maintained at the breakdown voltage plus the standard overvoltage throughout the experiment. The standard overvoltage values are provided by Hamamatsu: 2.7 V for S14160-3050HS and 3 V for S14520-3050VS.

### 2.1.2 Pre-amplifier circuit

The output signal of the SiPM is a charge pulse. We used a 50-Ω shunt resistor to convert this signal to a voltage pulse, followed by a 30-dB pre-amplifier to provide a larger amplitude signal for readout. The 30-dB pre-amplifier design is based on the monolithic microwave integrated circuit low-noise amplifier INA02186<sup>15</sup> and gives a flat gain up to 1 GHz with a simple circuit design. The SiPM is AC coupled to this pre-amplifier with each detected single-photon yielding photoelectrons (PE) that produce a ~5-mV peak output.

**Table 2** NUTTelA-TAO specifications.

Diameter of primary mirror	0.7 m
Central obstruction	47% of primary mirror diameter
Focal length	4540 mm (F6.5)
Effective light collection area	2.998 m <sup>2</sup>
Optimal field of view	70 mm (0.86°)
Image scale	22-μm per arc sec

### 2.1.3 Data logging setup

In the experiment, an MSO4104C Tektronix oscilloscope was used for data logging.<sup>16</sup> To simulate our proposed next-generation data logging scheme, we limited the sampling rate of the oscilloscope to 100 megasamples per second (100 Msps) with a bandwidth of 20 MHz, which is similar to common analog-to-digital converter (ADC) data acquisition systems. The oscilloscope memory allowed us to take  $2 \times 10^7$  data points for each measurement, corresponding to 0.2-s observation time on each target under 100-Msp sampling rate.

## 2.2 Telescope Specifications

The NUTTelA-TAO telescope (Fig. 1) and instrumentation are described in Ref. 9. The telescope has two Nasmyth focus ports, one occupied by the Burst Simultaneous Three-Channel Instrument (BSTI), so we mounted our instrument on the second port. The specifications of the telescope are given in Table 2.

Our SiPMs have a single channel of 3 mm × 3 mm active area which views 2.2716' × 2.2716' at the NUTTelA-TAO Nasmyth focus under 4540-mm focal length.

## 3 Observation Details

We performed measurements on two consecutive nights, each with a different detector. Our list of observed targets and experimental conditions for each night are given below.

### 3.1 October 28, 2019: Measurements with SiPM S14160-3050HS

On the first night of the test, the sky was slightly cloudy with a humidity of 60% and a sky temperature of -25°C. We chose to observe stars near zenith to minimize atmosphere effects. A dark portion of the sky (dark sky) with no source brighter than 18 mag is also observed. Observations were made with SiPM S14160-3050HS, with sensor temperature of -2.3°C to -2.5°C. The observation log is given in Table 3.

**Table 3** Measured data from SiPM S14160-3050HS.

Target	Brightest star mag (Gaia G-band)	Calibrated flux (Gaia G-band, e <sup>-</sup> s <sup>-1</sup> )	SiPM counts in 200 ms	Crosstalk (%)	Data
Star field	+7.93	12,563,646	341,726	23.2	Fig. 18
Star field	+10.89	875,522	78,615	13.61	Fig. 19
Star field	+13.11	121,332	63,231	13.08	Fig. 20
Star field	+14.91	26,911	58,415	12.82	Fig. 21
Dark sky	> + 18	3,542	53,769	12.57	Fig. 22
Dark test	\	\	16,988	10.72	Fig. 23

**Table 4** Observation log for October 28, 2019.

Target	Coordinate of pointing (J2000)	Brightest star mag (Gaia G-band)	Observe time (local: GMT+6)	Airmass
Star field	RA 6 h 51 m 11.11 s, DEC 58° 25' 2.8"	+7.93	04:24(+1d)	1.05
Star field	RA 6 h 50 m 54.42 s, DEC 58° 23' 5.7"	+10.89	04:28(+1d)	1.04
Star field	RA 6 h 56 m 49.31 s, DEC 58° 21' 36.5"	+13.11	04:32(+1d)	1.04
Star field	RA 6 h 56 m 40.19 s, DEC 58° 28' 53.4"	+14.91	04:36(+1d)	1.04
Dark sky	RA 6 h 56 m 12.07 s, DEC 58° 39' 26.2"	> + 18	04:40(+1d)	1.04
Dark test	Dark count testing (shutter closed)	\	04:45(+1d)	\
Star field	RA 6 h 53 m 3 s, DEC 59° 26' 53.8"	+5.2 (saturated)	04:56 (+1d)	1.04

### 3.2 October 29, 2019: Measurements with SiPM S14520-3050VS

On the second night, we changed to SiPM S14520-3050VS. The sky was clearer, with a sky temperature of  $-28^{\circ}\text{C}$ . The SiPM temperature was  $+2.4^{\circ}\text{C}$  to  $+2.6^{\circ}\text{C}$ . We measured the same set of stars and dark sky as the previous night, but at greater airmass due to observing the field at a different time of night. The observation log is given in Table 4.

## 4 Data Processing and Reduction

### 4.1 Noise Reduction and Baseline Cancellation

The observatory power supply system produces frequent voltage spikes with frequencies  $>10$  MHz. Our pre-amplifier was powered from this source; the residual voltage spikes are the dominant source of noise in our data. We used a 21-point Savitzky–Golay low-pass filter to reduce this noise while preserving the area under the data pulse, which varies with frequencies  $<10$  MHz. This filter limits our timing resolution to  $\sim 100$  ns. Another noise source in our data is baseline drift, which comes from AC to DC power converters and is low frequency, mainly  $<100$  Hz. We apply a 200-point moving mean filter with a high pass cut-off frequency of 500 kHz, and then subtract this smoothed baseline from the data to eliminate this drift.

The SiPM pulse has a sharp rise and a long decay tail of around a hundred ns. When multiple photons arrive within the decay (tail) time, pile-up occurs. To correct for pile-up, the start point of each pulse is adjusted to zero to ensure an accurate measurement. Figure 2(a) shows part of the raw data measured using the S14520-3050VS SiPM and Fig. 2(b) shows the processed data after noise reduction and baseline cancellation.

### 4.2 Photoelectron Identification

As mentioned before, SiPMs have a constant photon gain under constant overvoltage.<sup>10</sup> Therefore, the output charge ( $C = \int Idt$ ) should give the number of arrival photons.

In our shunt and pre-amplifier electronics, the charge is converted to a voltage pulse, and ideally, the time integral of the pulse gives the number of detected photons over the integration. We, therefore, performed a trapezoid integration of each voltage pulse, and recorded the arrival time.

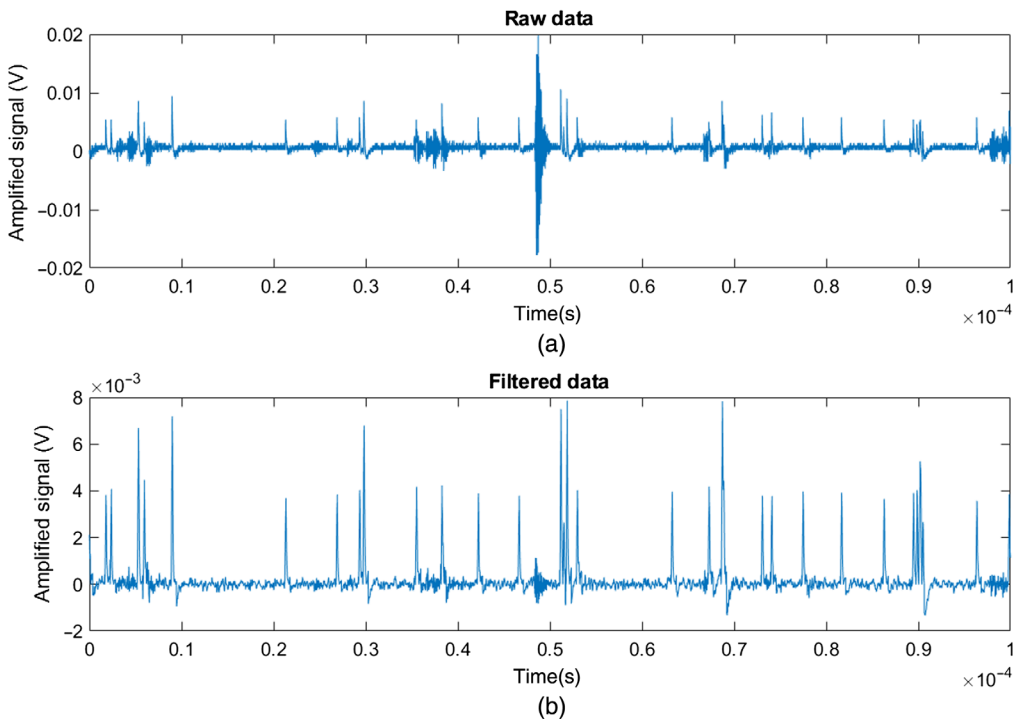


**Fig. 2** (a) Raw data, measured with S14520-3050VS. (b) Processed data, after filtration and baseline cancellation.

Ideally, the pulse area histogram should be in discrete steps (as fractional photons are unphysical). In reality, the amount of calculated charge under each pulse can be affected by the electronic noise, imperfect pile-up correction, variation in the sensor, and readout system rounding errors. Each discrete pulse level then becomes broadened into a Gaussian distribution, and so the overall pulse area histogram becomes a sum of Gaussians.<sup>17,18</sup> To reduce these effects and correctly calculate the number of arrival photons, we implement a two-step Gaussian mixture model (GMM) with the steps below.<sup>19</sup>

1. We fit a two-peak GMM distribution to the data using an iterative expectation-maximization (EM) algorithm with a starting guess generated from a “k-means++” algorithm, which then generates a starting point by nearest mean clustering.<sup>20,21</sup> This algorithm provides us with the centroid and variance of the first and second PE peaks (i.e., 1 PE and 2 PE).
2. From the centroid and variance of the first and second peaks, we estimate the centroid and variance of other PE peaks of the charge distribution using a linear regression forecast.
3. Having estimated values for the center and variance of each PE peak, we perform GMM fitting again to obtain the precise number of arrival photons.

We applied this second step of GMM fitting because the first auto GMM fitting did not provide precise information about peaks for  $>2$  PE.

### 4.3 Saturated Data

Bright illumination of the SiPM causes saturation when the SiPM output pile-up occurs at a level such that single pulses can no longer be distinguished. In this case, the SiPM can still accept more photons, but we can not identify them on a photon-counting basis. Figure 3 shows this case when we were observing 14 Lyn (a star with G-band magnitude of 5.2).

From Fig. 4, we can see that the GMM algorithm for photon number cannot be applied. By comparing Figs. 4 and 5, we find that the algorithm is not working well as 1 PE and 2 PE overlaps and they are not distinguishable from each other.

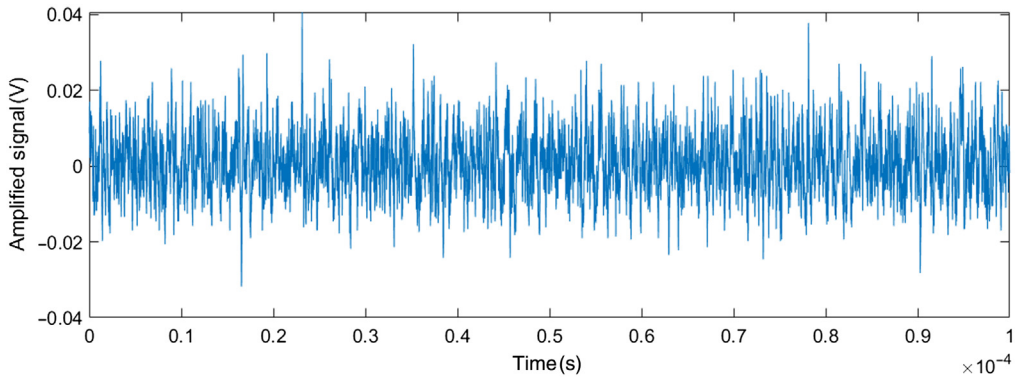


**Fig. 3** Saturated data from measurement of the bright star 14 Lyn using SiPM S14520-3050VS.

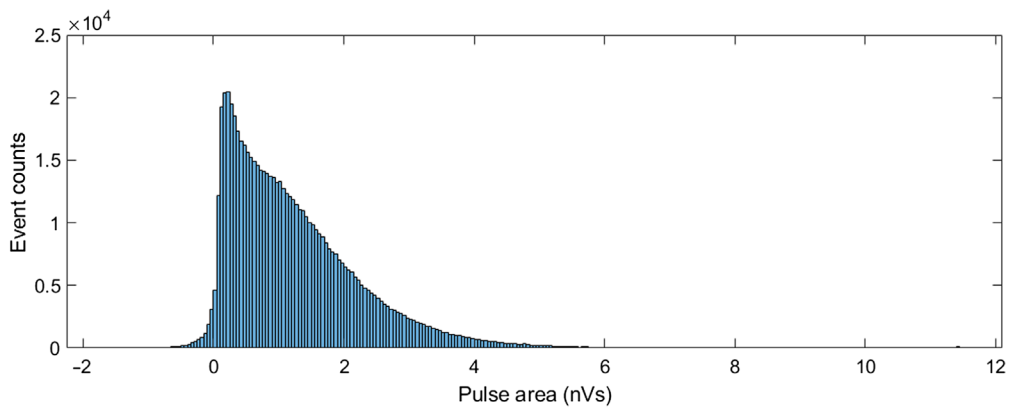


**Fig. 4** Histogram plot of the saturated data from Fig. 3.

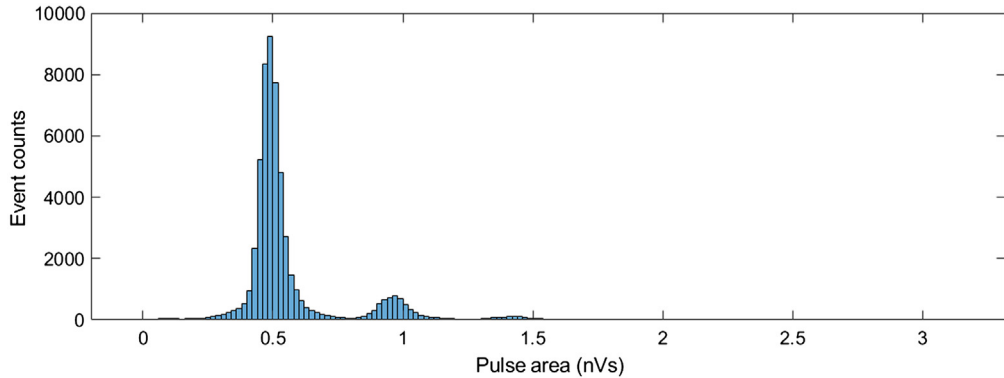


**Fig. 5** A histogram plot of pulse area of different photon pulses. It is noteworthy that the first and second peaks are both Gaussian-like, motivating the GMM used for fitting.

#### 4.4 Crosstalk Measurement

As mentioned above, when crosstalk occurs, one input photon will produce a two or higher PE pulse, which is indistinguishable from a real multiple PE signal.<sup>22</sup> Below, we find that crosstalk limits our ability to measure transient signals at very short time scales. We, therefore, need to measure the crosstalk as a function of count rate for our devices.

Measured crosstalk increases linearly with total count rate, with a zero-point, the “intrinsic crosstalk”:

$$\begin{aligned} \text{Measured cross talk rate} &= \text{intrinsic cross talk} + \text{multi-P.E. illumination cross talk rate} \\ &= \frac{\text{> 1 P.E. SiPM count}}{\text{total count rate}} \end{aligned} \quad (1)$$

(We demonstrate this linearity in the Sec. 5.) To determine the crosstalk for any given count rate, we analyze data with a range of multi-PE illumination and fit the intrinsic rate and slope of the function for each device. (Here, we assume our illumination source is constant, so the number of multiple PE peaks (>1 PE) grows linearly with the flux (within expected fluctuations from Poisson statistics). The results of these fits are given below.

## 5 Data Analysis

Our SiPMs are sensitive in the range of 300 to 900 nm, similar but more blue-biased compared to the Gaia Data Release 2 (DR2) G-band passband.<sup>22,23</sup> To flux calibrate our data, we, therefore, compared our results with the standard G-band flux data from the Gaia satellite DR2 archive.<sup>22,23</sup> The DR2 G-band passband is shown in Appendix A Fig. 15.

Our photometry analysis assumes integration over a circular aperture (diameter 2.563') of the same field of view as our detection field.

### 5.1 SiPM S14160-3050HS

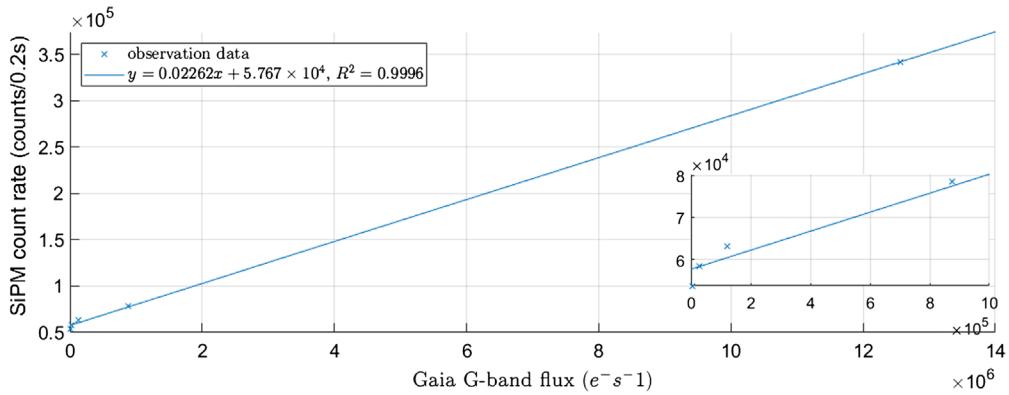
On the first night, we used the SiPM S14160-3050HS (See Tables 1 and 3). We corrected for airmass effects on our count rate for our photon flux calibration.<sup>24</sup> Table 5 shows the calibrated flux, measured SiPM counts from stars, dark counts, and calculated crosstalk rate (saturated data are not listed). The analyzed data are presented in Appendix C, Figs. 18–23.

Figure 6 shows the airmass-corrected count rate versus the calibrated G-band flux.

The zero-flux intercept in Fig. 6 gives dark counts plus sky background within a 200-ms window, 57,670 counts. We measured a SiPM dark count rate of ~85 kilocounts per second (kcps; Table 5). This gives a sky background of ~203 kcps.

**Table 5** Observation log for October 29, 2019.

Target	Coordinate of pointing (J2000)	Brightest star mag (Gaia G-band)	Observe time (local: GMT+6)	Airmass
Star field	RA 6 h 53 m 3 s, DEC 59° 26' 53.8"	+5.2 (saturated)	23:17	1.71
Star field	RA 6 h 51 m 11.11 s, DEC 58° 25' 2.8"	+7.93	23:21	1.66
Star field	RA 6 h 50 m 54.42 s, DEC 58° 23' 5.7"	+10.89	23:24	1.64
Star field	RA 6 h 56 m 49.31 s, DEC 58° 21' 36.5"	+13.11	23:27	1.66
Star field	RA 6 h 56 m 40.19 s, DEC 58° 28' 53.4"	+14.91	23:31	1.64
Dark sky	RA 6 h 56 m 12.07 s, DEC 58° 39' 26.2"	> + 18	23:35	1.62
Dark test	Dark count testing (shutter closed)	\	23:39	\



**Fig. 6** SiPM airmass-corrected counts in 0.2 s versus calibrated G-band flux for SiPM s14160-3050HS. Inset gives data at low count rate.

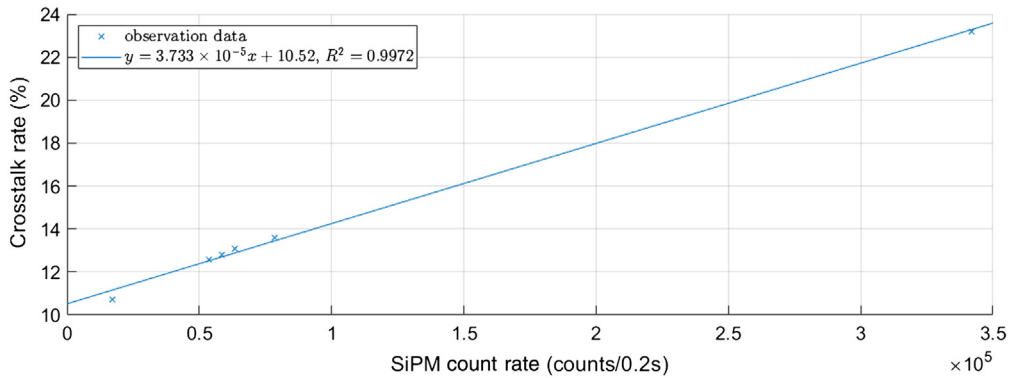


**Fig. 7** Fit of measured crosstalk versus airmass-corrected count counts in 0.2 s for SiPM s14160-3050HS.

From the zero-flux intercept, and its uncertainty  $\sigma_{\text{intercept}} = \sqrt{57670} = 240$  counts in 200 ms, we can calculate the  $5\sigma$  sensitivity to be 1200 counts, corresponding to a Gaia G-band flux of  $53,050 e^- s^{-1}$ , equivalent to a 13.9 G-band mag point source (assuming no atmospheric extinction). If we increase the integration time to 1 s, the SNR scales  $\sqrt{t}$ , giving a  $5\sigma$  detection limit of 14.7 G-band mag in 1 s.

Figure 7 shows the fit of measured crosstalk versus count rate. We measured the intrinsic or zero-point crosstalk of SiPM S14160-3050HS to be 10.52%.

## 5.2 SiPM S14520-3050VS

On the second night, we used SiPM S14520-3050VS (see Tables 1 and 4). We carried out the same measurements as on the first night, with results given in Table 6. The analyzed data are presented in Appendix D, Figs. 24–29.

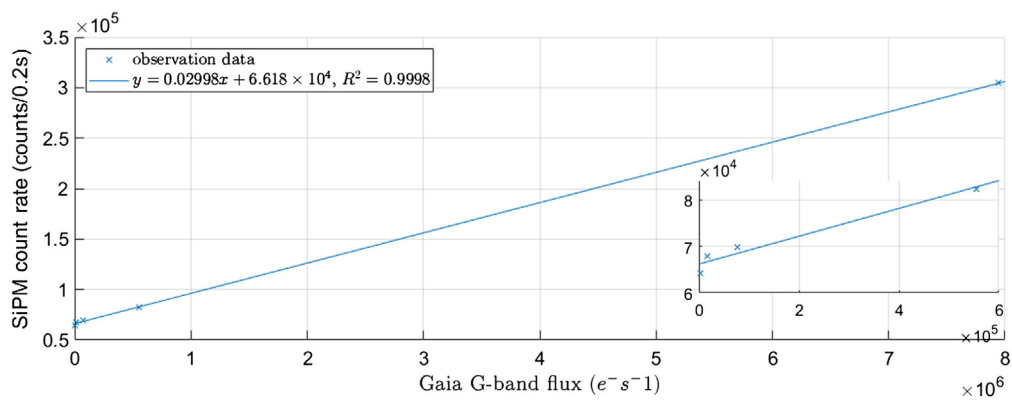
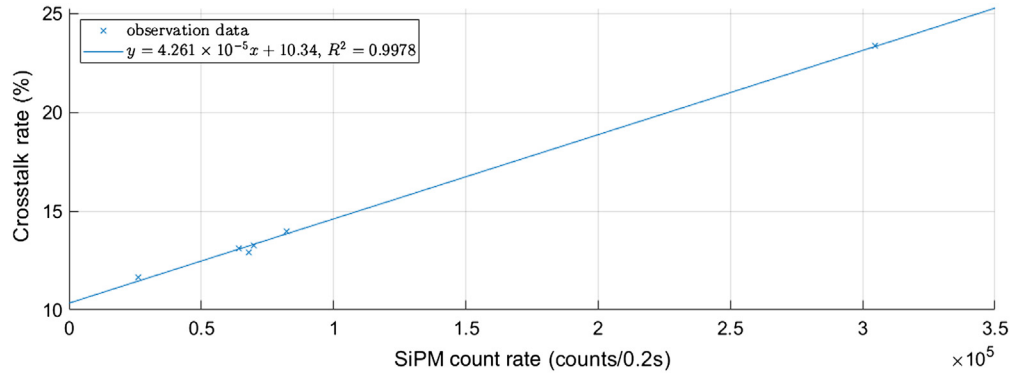
Figure 8 shows SiPM count rate versus calibrated G-band flux.

From Fig. 8, and Table 6, the SiPM dark count rate is  $\sim 130$  kcps while the sky background is  $\sim 201$  kcps (after subtracting the dark counts). As above, from  $\sigma_{\text{intercept}} = 248$  counts, we find the  $5\sigma$  sensitivity to be 1240 counts within 200 ms, corresponding to a Gaia G-band flux of  $41,361 e^- s^{-1}$ , or a 14 G-band mag point source detected in 200 ms (assuming no atmospheric extinction). Scaling by  $t^{-1/2}$  gives a detection limit of 14.9 G-band mag in 1 s.

Figure 9 shows the fit of the measured crosstalk versus count rate, giving an intrinsic cross-talk for SiPM S14520-3050VS of 10.34%.

**Table 6** Measured data from SiPM S14520-3050VS.

Target	Brightest star mag (Gaia G-band)	calibrated flux (Gaia G-band, $e^- s^{-1}$ )	SiPM counts in 200 ms	Crosstalk (%)	Data
Star field	+7.93	7,946,884	304,481	23.34	Fig. 24
Star field	+10.89	555,209	82,317	13.94	Fig. 25
Star field	+13.11	76,015	69,858	13.27	Fig. 26
Star field	+14.91	17,065	67,854	12.9	Fig. 27
Dark sky	> + 18	2,274	64,171	13.11	Fig. 28
Dark test	\	\	26,103	11.65	Fig. 29

**Fig. 8** SiPM airmass-corrected counts in 0.2 s versus calibrated G-band flux for SiPM S14520-3050VS. Inset gives data at low count rate.**Fig. 9** Measured crosstalk versus airmass-corrected count counts in 0.2 s for SiPM S14520-3050VS.

### 5.3 Time Domain Analysis

A prime motivation for our use of a SiPM detector is the ability to resolve events at short time scales. During all our observations of stars, no significant change in brightness was measured, as expected. We applied both 10  $\mu$ s and 1 ms moving mean filters to produce smoothed light curves for all observations. These light curves, together with the histogram plot of photon statistics and corresponding Gaia star chart of each observation, are attached in the Appendix C and D.

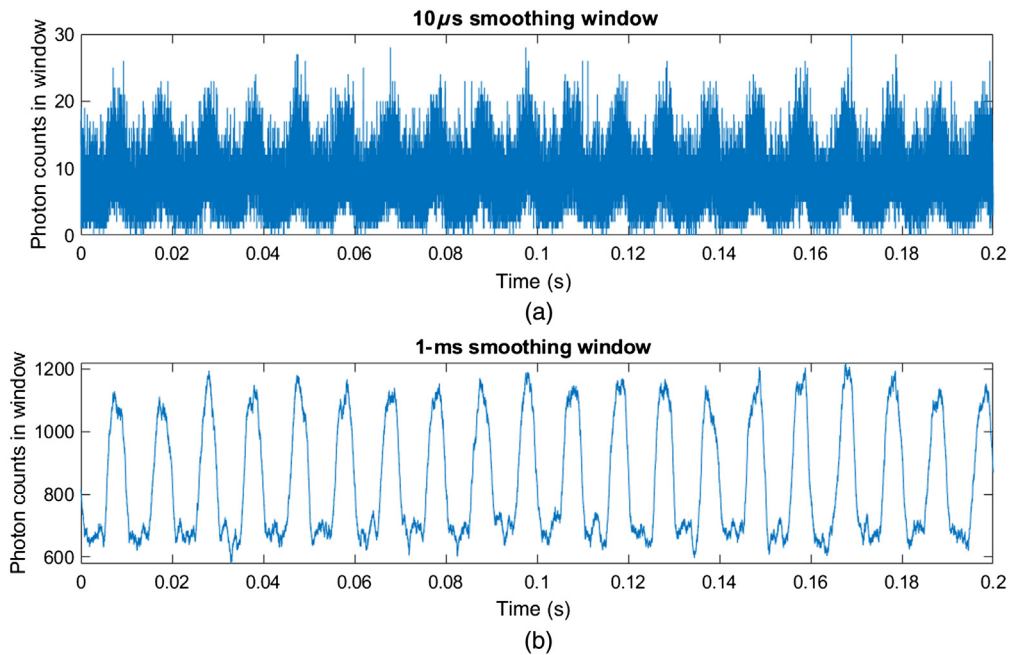


**Fig. 10** (a)  $10\ \mu\text{s}$  and (b) 1 ms smoothed signal from artificial 100-Hz scattered square wave light.

### 5.3.1 Synthetic light source test

To simulate the response of our detectors to a fast transient signal, we scattered an artificial light source with a  $\sim$ 100-Hz square wave modulation into the telescope in the middle of our observations.

In Fig. 10, the 100-Hz signal data are shown using moving-mean filters with  $10\ \mu\text{s}$  and 1 ms windows. The 1-ms window gives much better SNR compared to  $10\text{-}\mu\text{s}$  as expected. The spectrum of the light source is attached in Fig. 11 measured by a AvaSpec-2048 spectrometer with background removal.

### 5.3.2 Sensitivity versus time scale

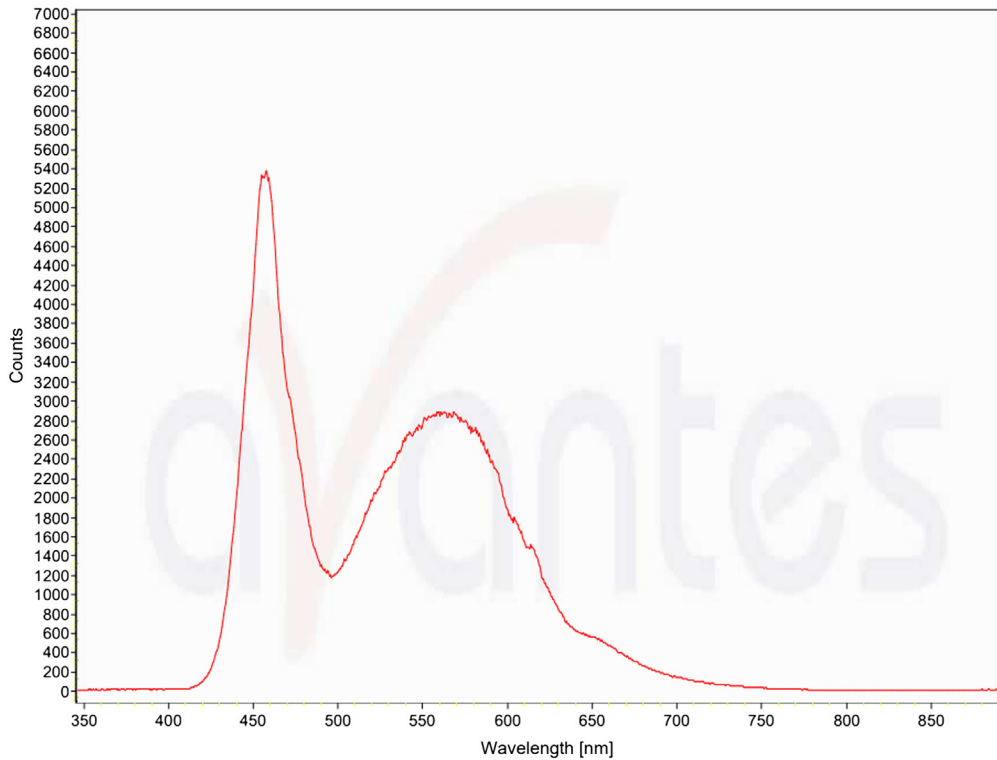
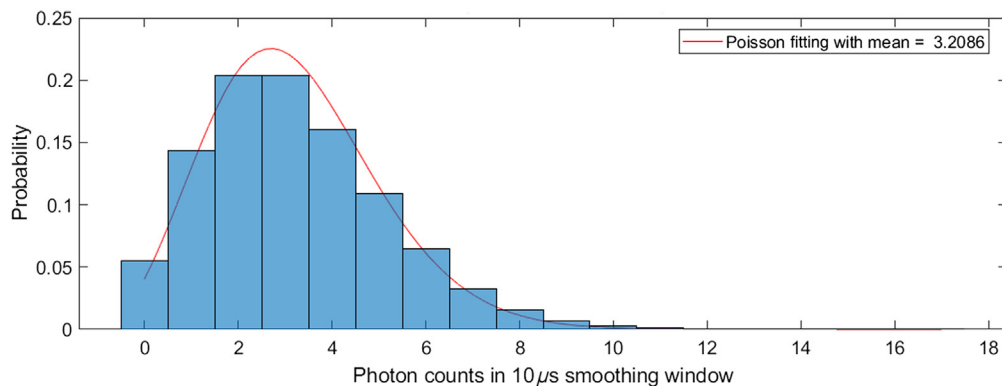
Here, we derive our detection limits for fast transients at various time scales. If we consider a dark portion of the sky, what is the minimum brightness of transient that we can detect?

Consider the measured dark sky using detector model S14520-3060VS, as given in Table 4 and 6, we measured 64,171 photons within 200 ms.

For fast transients, we measure only small numbers of photons and therefore need to consider shot noise (Poisson fluctuations); we are not in the Gaussian regime. We, therefore, fit the data to a Poisson distribution:

From Fig. 12, for SiPM S14520-3050VS, we find that the mean photon count rate is 3.2086 per  $10\ \mu\text{s}$ . If we select a desired false alarm rate of  $<1$  event per 100 night ( $\sim 5 \times 10^6$  s), we would then need a false trigger rate of  $<1$  per  $5 \times 10^{11}$  time bins. From simple Poisson statistics, this corresponds to a detection threshold of 22 photons detected within  $10\ \mu\text{s}$ . Comparing to the above count rate versus calibrated G-band flux (Fig. 8), the transient should give a G-band flux of at least  $\sim 7.6 \times 10^7 e^- \text{ s}^{-1}$  ( $\sim 6$  G-band mag) in the  $10\text{-}\mu\text{s}$  bin. Even for a false alarm rate as high as 1 event per night, we still need 20 photons detected within  $10\ \mu\text{s}$ , or  $\sim 6.9 \times 10^7 e^- \text{ s}^{-1}$  ( $\sim 6.1$  G-band mag) in the  $10\text{-}\mu\text{s}$  bin.

Consider nanosecond time scale transients and a false alarm rate  $\ll 1$  false alarm per 100 nights. From the same dark sky observation, we have 64,171 photons detected in 200 ms (Tables 4 and 6) which corresponds to  $1.5 \times 10^{12}$  photons per 100 nights. In nanosecond time bins, photons will pile up, and be detected as a multi-PE event. Such events have a low occurrence rate in the absence of crosstalk. For example, we got 64,171 photons detected in 200 ms,

**Fig. 11** Spectrum of the 100-Hz artificial light source used.**Fig. 12** Poisson fit to SiPM measurement of dark sky.

correspond to one photon per  $\sim 3 \mu\text{s}$ . If we consider the SiPM decay (tail) time of 100 ns, then the natural rate of concurrent photons received is just  $100 \text{ ns} / 3 \mu\text{s} = 3\%$ . However, the measured crosstalk (which counts also the natural photons pile up) is 13.11%, much higher than 3%. This limits our sensitivity for nanosecond time scale transients.

To maintain one false alarm per 100 nights, less than one event should go above threshold among all  $1.5 \times 10^{12}$  photons detected, i.e., trigger probability  $< 1 / 1.5 \times 10^{12}$ . With measured crosstalk of 13.11%, we should require  $(13.11\%)^N \leq 1 / 1.5 \times 10^{12}$ , where  $N$  is the trigger threshold in number of photons. Solving gives a trigger threshold of least 14 PE. Considering an average SiPM detection efficiency of  $\sim 30\%$  over 300- to 900-nm range and collection area  $0.2998 \text{ m}^2$  of the NUTTelA-TAO system, this gives a fluence threshold of 155 photons per square meter within nanoseconds.

## 6 Future Improvements and Plans

For either model of SiPM, we can detect stars brighter than  $\sim 14$  mag in 200-ms bins, and saturation occurs at  $\sim 7$  mag. To perform astrophysical measurements for fast transient events, we need to have a higher dynamic range. For example, the Crab Pulsar PSRB0531 + 21 itself is a 16.5-V-band magnitude source embedded in an 8.4-V-band magnitude nebula.<sup>25</sup> Therefore, we need to improve our ability to measure a faint point source against a bright nearby background.

Currently, the SiPM sensitivity and dynamic range are mainly limited by spatial resolution. Our sky background is  $\sim 200$  kcps for both detectors. A sensor with smaller physical size would have a significantly lower background rate. If the sensor were to view  $10'' \times 10''$ , the equivalent sky noise would be reduced by 185 times, a roughly 5.7 magnitude improvement. The same improvement would be achieved in dark count rate, since this scales with sensor area. Therefore, we aim to have a much smaller SiPM-based detector in our next iteration.

Both SiPMs have higher intrinsic crosstalk than the manufacturer's specifications (10.52% versus 7% for S14160-3050HS and 10.34% versus 5% for S14520-3050VS). Possible causes include internal reflections from mounts and telescope mirrors, or a thin layer of frozen moisture on the sensor surface which we discovered on daytime inspection after the observation nights. We intend to pursue reduction of these possible causes.

To improve our readout system, we are in the process of developing a standalone field-programmable gate array (FPGA)-based system.<sup>26,27</sup> We are planning to use a system-on-chip FPGA with an integrated ARM core to host a linux-based system. The SiPM signal should be converted to digital data using a high-speed ADC, and then logged by the FPGA. The FPGA can then calculate the statistical significance of putative transients in real-time. If any candidate event is detected, the system could record the raw photon arrival information and alert the observer automatically to enable additional follow-up.

During this experiment, we observed strong noise from the observatory power supply. To remove the noise, we will develop an isolated power supply for the detectors and the analog readout system.

## 7 Conclusion

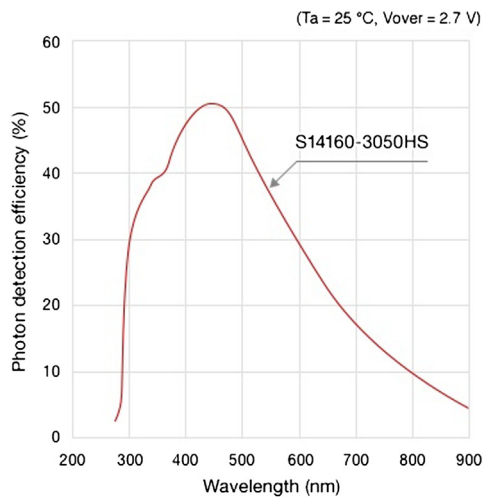
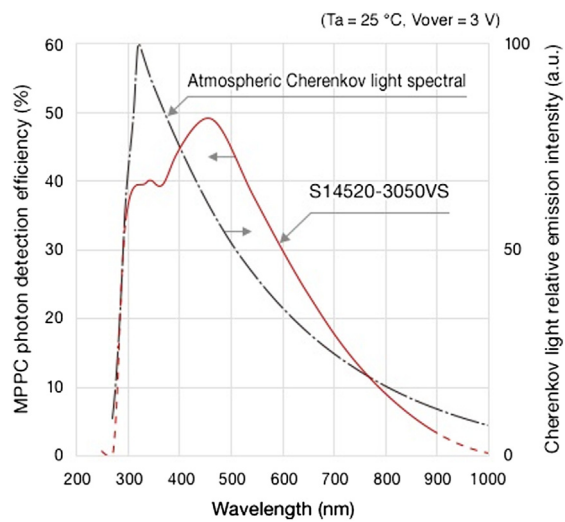
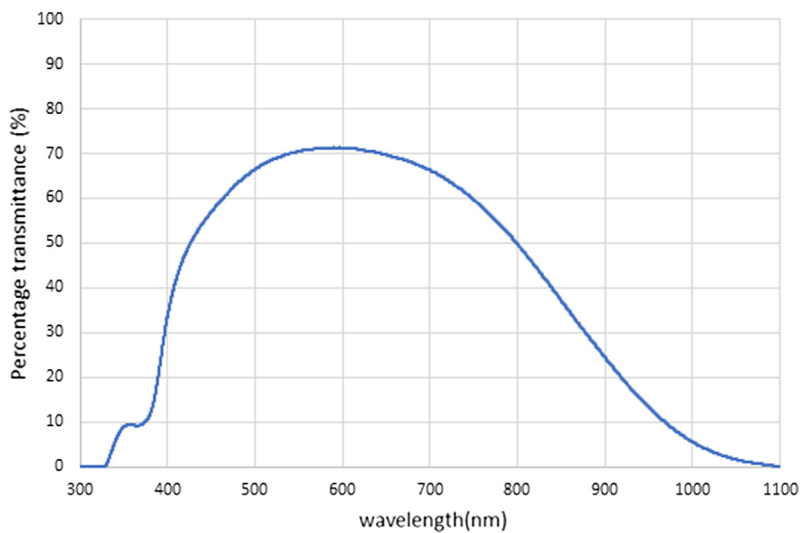
Initial measurements of two SiPM detectors for UFA have been successfully performed on the NUTTela-TAO telescope. The  $3\text{ mm} \times 3\text{ mm}$  SiPM sensors provide a detection limit of, respectively, 13.9 (S14160-3050HS) and 14 G-band mag (S14520-3050VS) in a 200-ms time window. The sky background and intrinsic crosstalk were measured to be  $\sim 201$ , 203 kcps and 10.34%, and 10.52% for the S14160-3050HS and S14520-3050VS model detectors, respectively. For a false alarm rate of once per 100 nights, the  $10\text{-}\mu\text{s}$  detection limit is 22 detected photons, which corresponds to a 6 G-band mag fast transient. At the shortest timescales, we derive a limiting fluence of  $\sim 155$  photons per square meter within 100 ns, limited by crosstalk. The crosstalk is higher than expected, possibly due to internal reflections or defects in our detectors. We plan to improve our system resolution by reducing the detector size, which reduces sky background and dark counts. Better astrophysical measurements should also be achieved by crosstalk and power supply noise reduction, readout electronics improvement to handle longer data streams. These changes will allow us to search for transients on short timescales in astrophysical applications which is the main goal of our UFA program.

## 8 Appendix A: SiPM models spectral response and Gaia G-band transmittance

Here, we report the spectral response of both models of SiPMs in Figs. 13 and 14. The Gaia G-band percentage transmittance in Data Release 2 is also reported in Fig. 15.

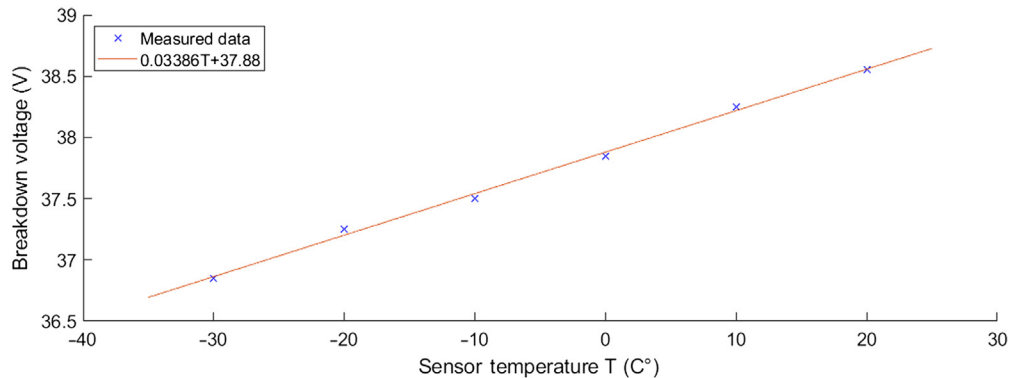
Figures 13 and 14: Credit to Hamamatsu photonics.

Figure 15: Reproduced with permission, courtesy of European Space Agency/Gaia/Data Processing and Analysis Consortium (DPAC).<sup>22,23</sup>

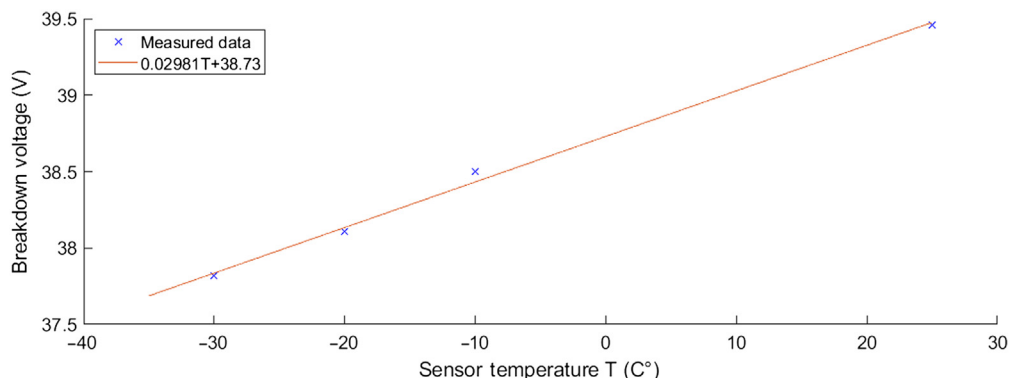
**Fig. 13** Hamamatsu SiPM S14160-3050HS spectral response curve.**Fig. 14** Hamamatsu SiPM S14520-3050VS spectral response curve.**Fig. 15** Passband of Gaia G-band in Data Release 2.

## 9 Appendix B: SiPM units breakdown voltage versus temperature calibration curves, tested in laboratory condition

Here, we report the breakdown voltage versus temperature calibration curves of the SiPM units used in Figs. 16 and 17. The tests are performed in laboratory condition.



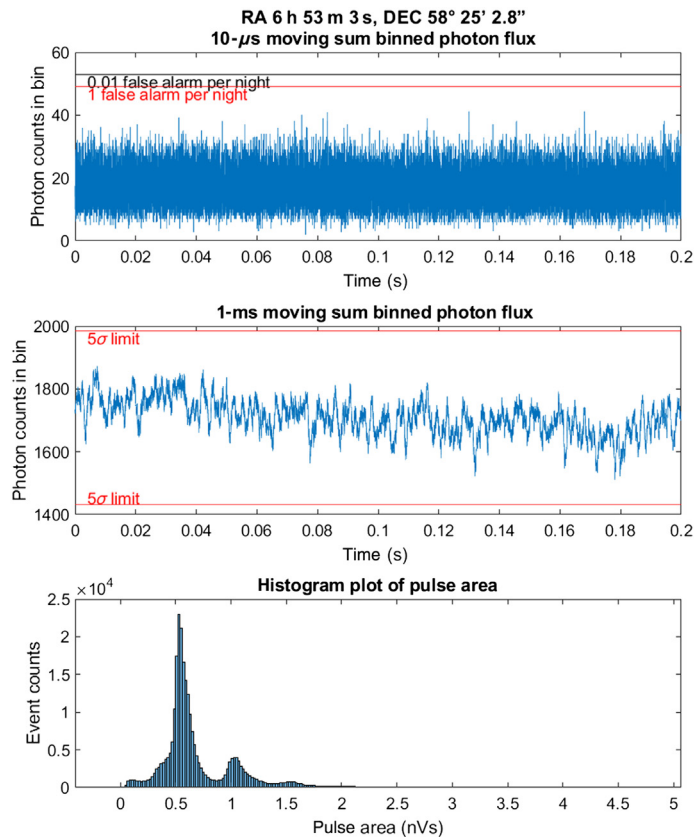
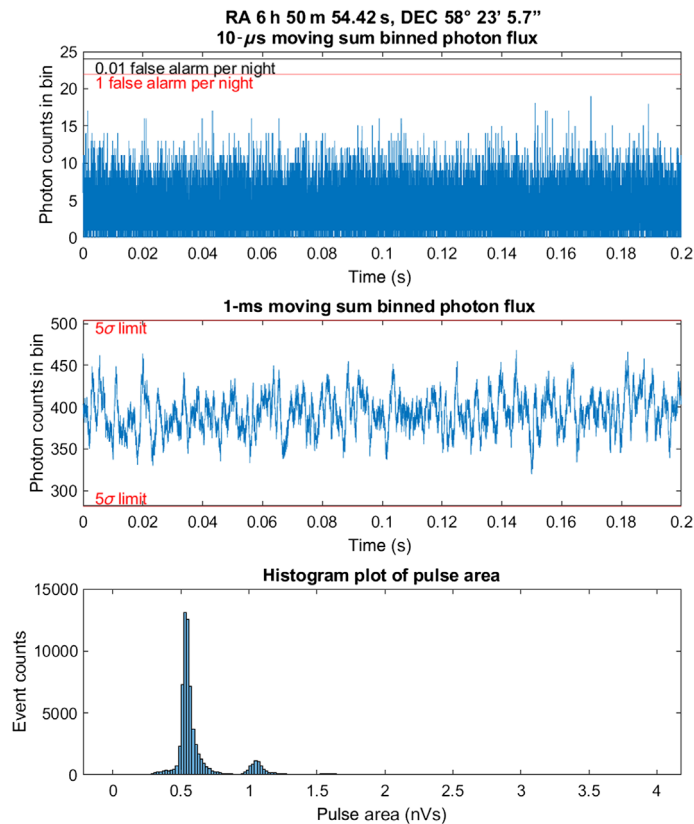
**Fig. 16** Hamamatsu SiPM S14160-3050HS breakdown voltage versus temperature calibration curve.

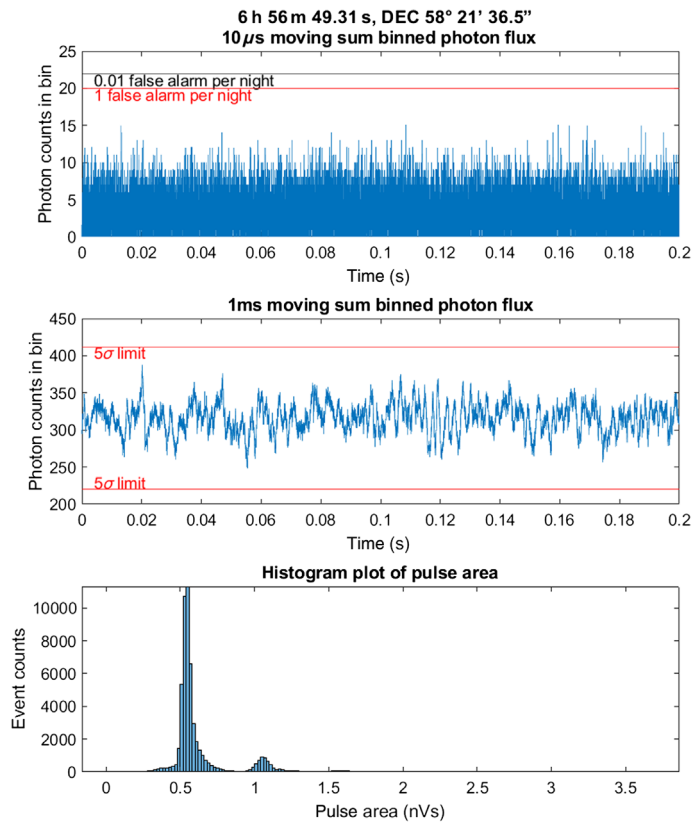
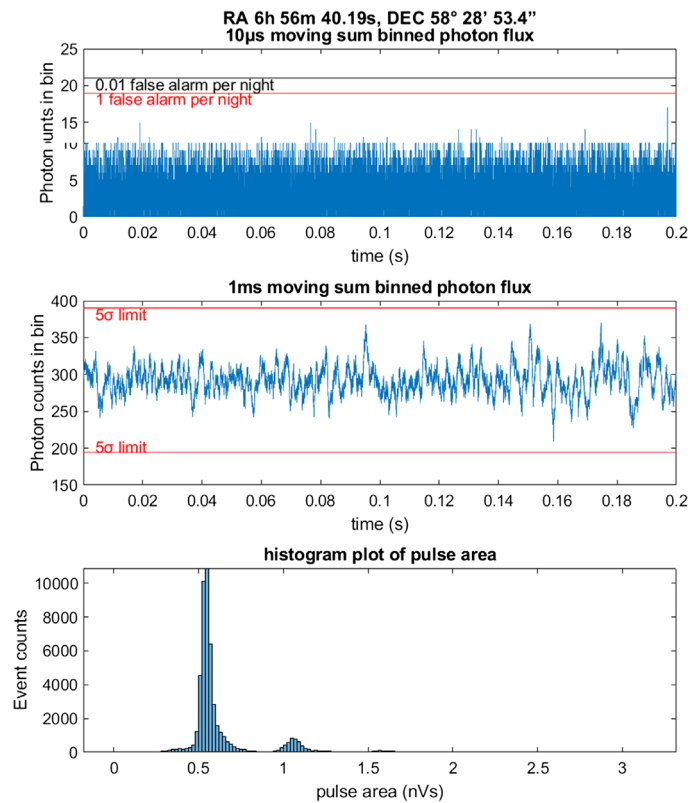


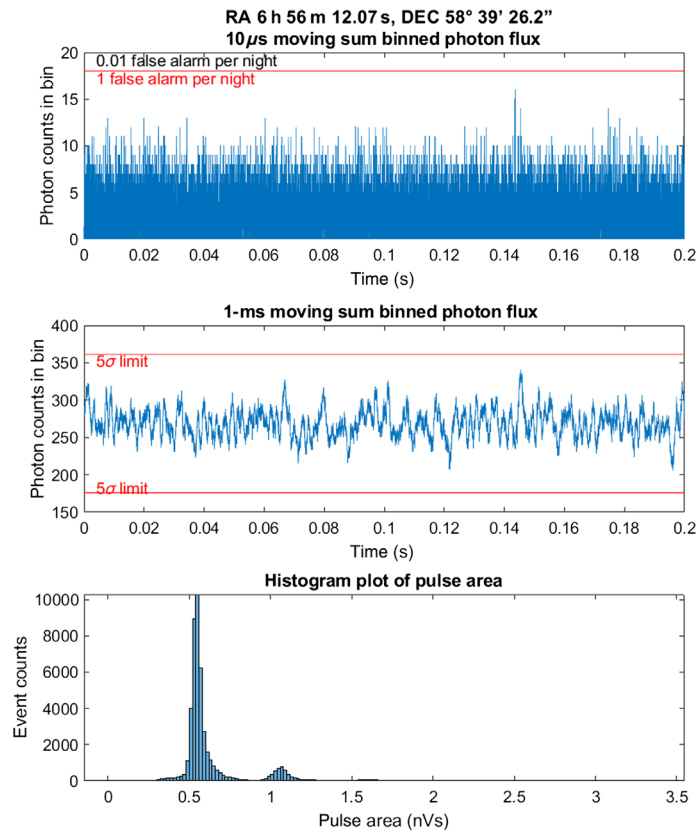
**Fig. 17** Hamamatsu SiPM S14520-3050VS breakdown voltage versus temperature calibration curve.

## 10 Appendix C: Analyzed Data from S14160-3050HS

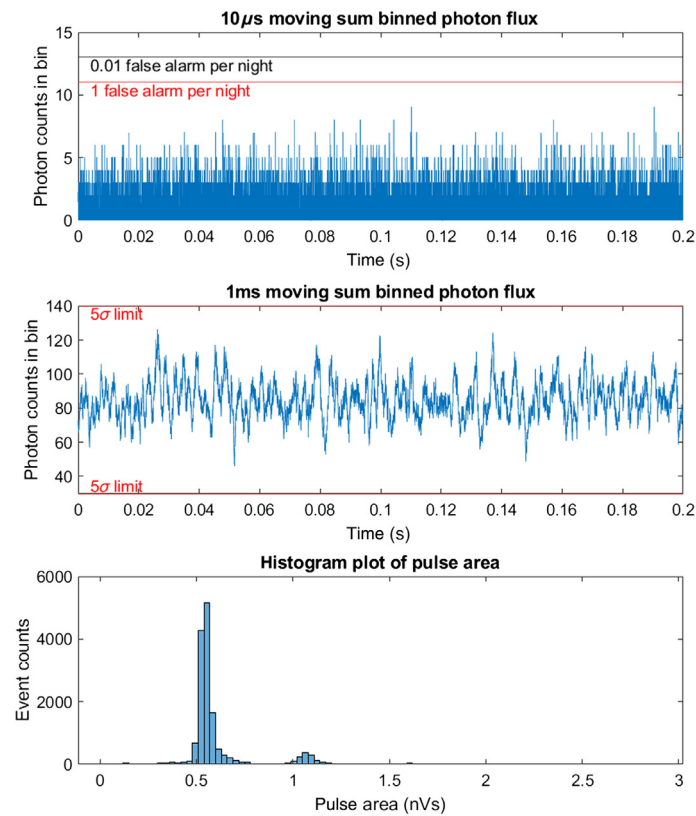
Here, we report the analyzed data from SiPM S14160-3050HS in Figs. 18–23.

**Fig. 18** SiPM S14160-3050HS observing HIP32890.**Fig. 19** SiPM S14160-3050HS observing a 10.89 mag (G-band) star.

**Fig. 20** SiPM S14160-3050HS observing a 13.11 mag (G-band) star.**Fig. 21** SiPM S14160-3050HS observing a 14.91 mag (G-band) star.



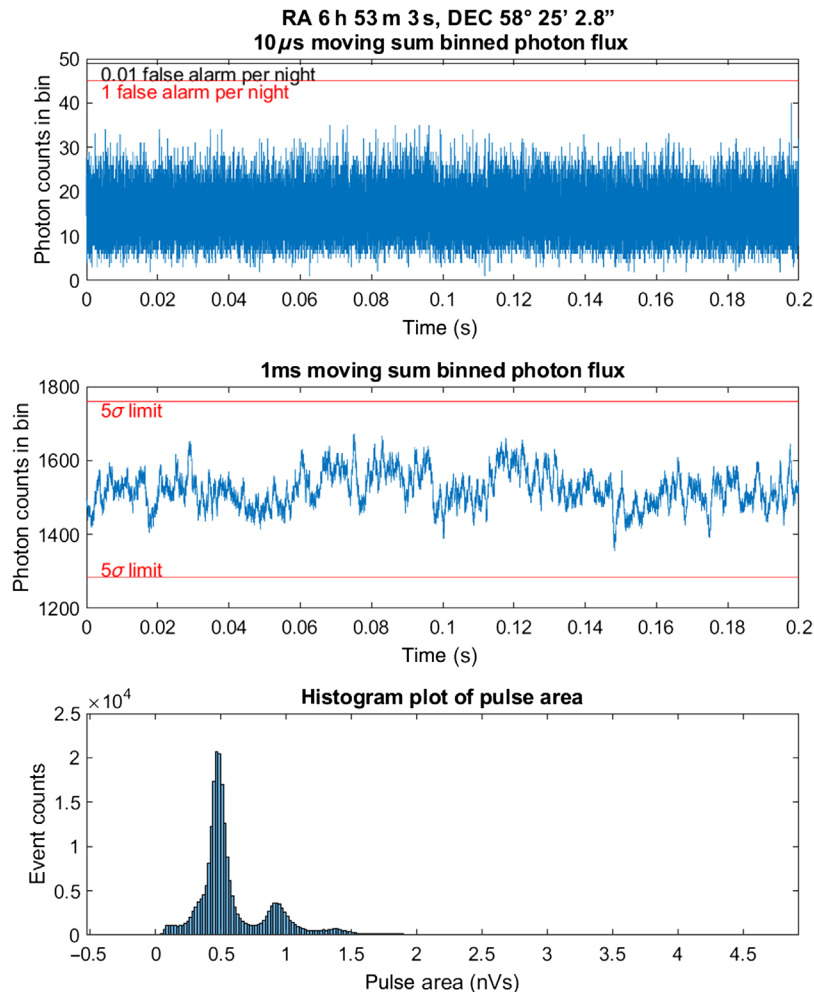
**Fig. 22** SiPM S14160-3050HS observing area without star brighter than 18 mag (G-band).



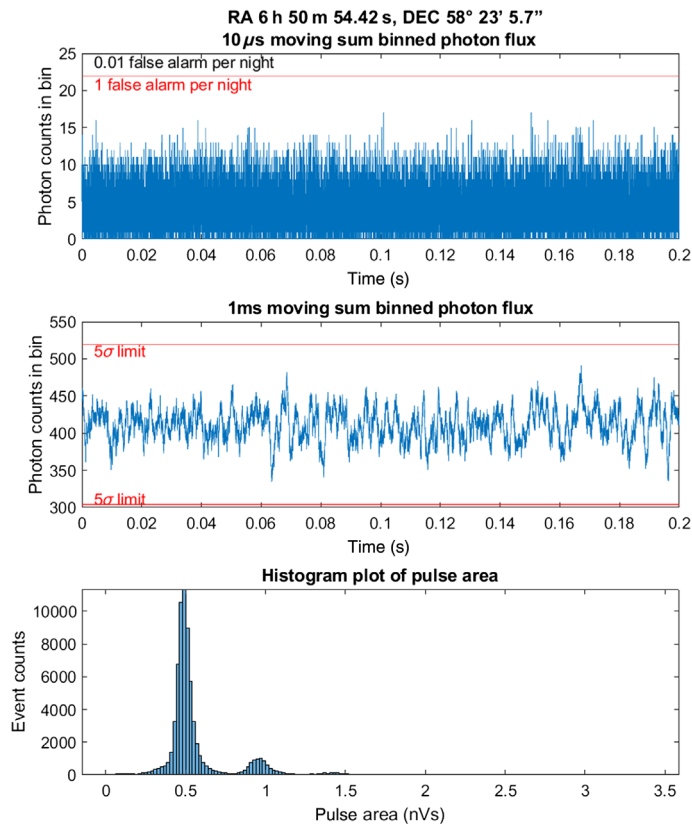
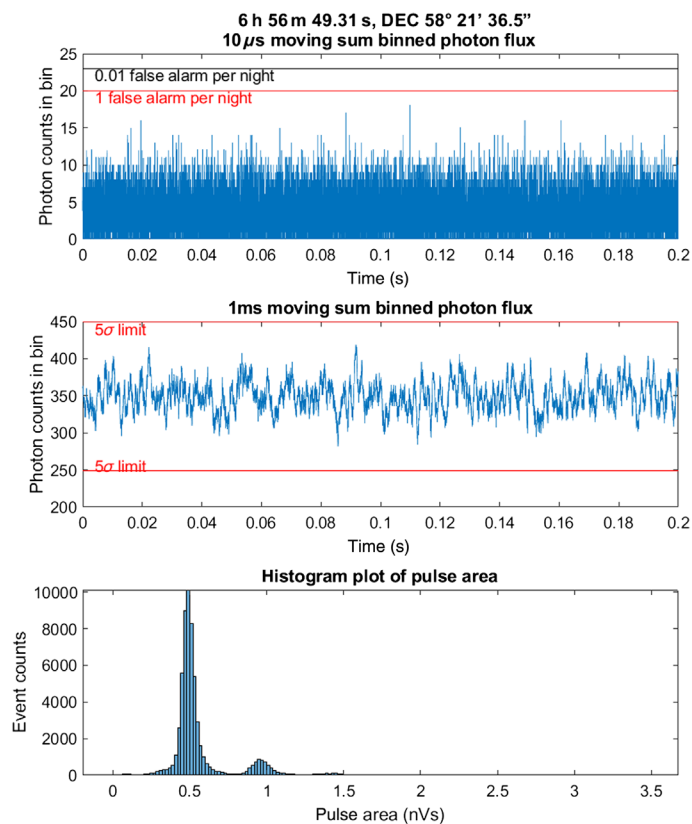
**Fig. 23** SiPM S14160-3050HS dark measurement on site.

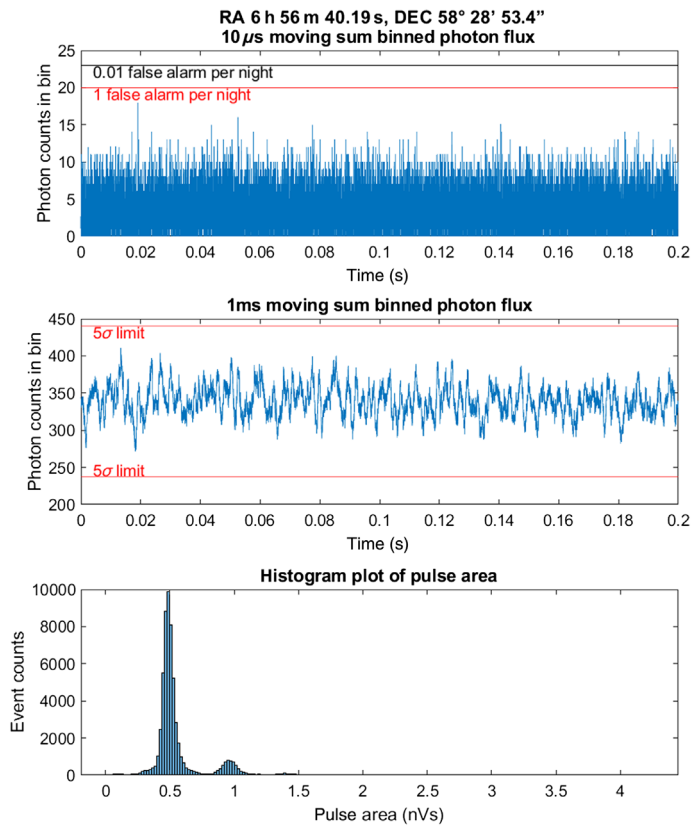
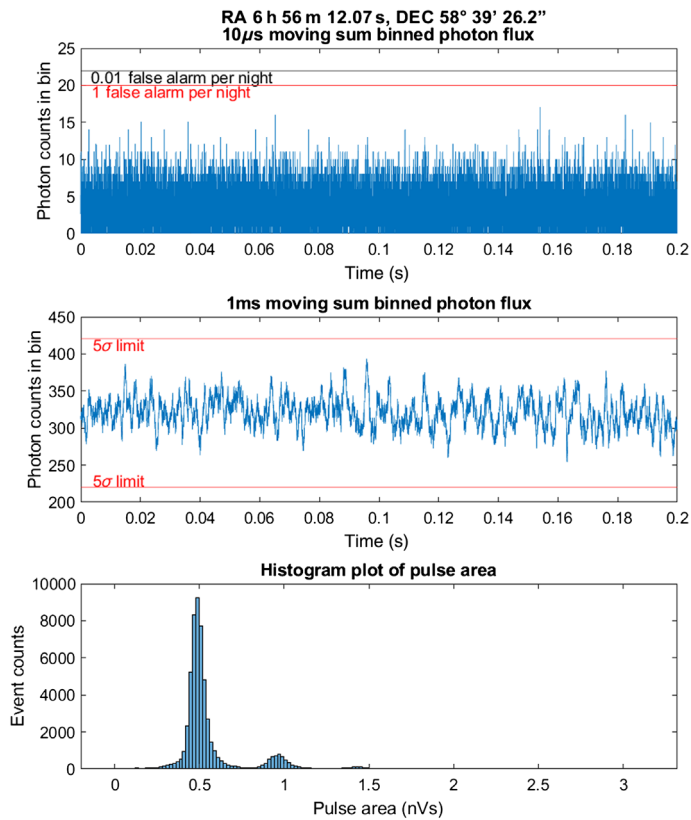
## 11 Appendix D: Analyzed Data from S14520-3050VS

Here, we report the analyzed data from S14520-3050VS in Figs. 24–29.



**Fig. 24** SiPM S14520-3050HS observing HIP32890.

**Fig. 25** SiPM S14520-3050HS observing a 10.89 mag (G-band) star.**Fig. 26** SiPM S14520-3050HS observing a 13.11 mag (G-band) star.

**Fig. 27** SiPM S14520-3050HS observing a 14.91 mag (G-band) star.**Fig. 28** SiPM S14520-3050HS observing area without star brighter than 18 mag (G-band).

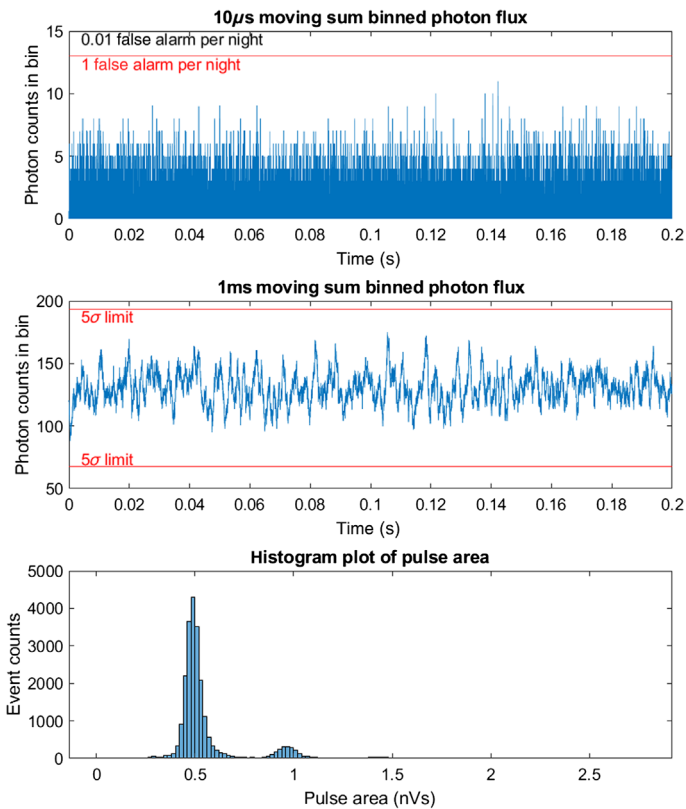


**Fig. 29** SiPM S14520-3050HS dark measurement on site.

## Acknowledgments

We acknowledge support from RK MES under grant No. AP05135753 through Nazarbayev University, Kazakhstan, and from the HKUST Jockey Club Institute for Advanced Study (IAS). We would like to offer special thanks to the staff of the Assy-Turgen Observatory and the Fesenkov Astrophysical Institute, especially engineer Maxim Krugov, for their support, help and advice during the experiment. We wish to acknowledge help in preparing the experiment by technicians Ulf Lampe and TK Cheng of the HKUST Physics Department. This work has made use of data from the ESA mission Gaia,<sup>28</sup> processed by the Gaia DPAC.<sup>29</sup> Funding for the DPAC has been provided by national institutions, in particular the institutions participating in the Gaia Multilateral Agreement.

## References

1. S. Li et al., “Program objectives and specifications for the ultra-fast astronomy observatory,” *Proc. SPIE* **11341**, 513–521 (2019).
2. L. K. Hardy et al., “A search for optical bursts from the repeating fast radio burst FRB 121102,” *Mon. Not. R. Astron. Soc.* **472**(3), 2800–2807 (2017).
3. A. Richichi et al., “Final binary stars results from the VLT Lunar Occultations Program,” *Astron. J.* **147**, 5 (2014).
4. W. Benbow et al., “Direct measurement of stellar angular diameters by the VERITAS Cherenkov telescopes,” *Nat. Astron.* **3**, 511–516 (2019).
5. M. Cossens et al., “Panoramic optical and near-infrared SETI instrument: prototype design and testing,” *Proc. SPIE* **10702**, 107025H (2018).
6. V. S. Dhillon et al., “HiPERCAM: a high-speed quintuple-beam CCD camera for the study of rapid variability in the universe,” *Proc. SPIE* **9908**, 99080Y (2016).
7. M. Shafee et al., “Design optimization of a 10 kilopixel optical band microwave kinetic inductance detector,” *J. Instrum.* **14**(12), P12011 (2019).

8. B. Alzhanov et al., “The cryogenic detector for cosmology observation,” *IOP Conf. Ser.: Mater. Sci. Eng.* **502**(1), 012060 (2019).
9. B. Grossan, P. Kumar, and G. F. Smoot, “The emission mechanism of gamma-ray bursts: identification via optical-ir slope measurements,” *J. High Energy Astrophys.* **23**, 14–22 (2019).
10. V. Saveliev, “The recent development and study of silicon photomultiplier,” *Nucl. Instrum. Methods Phys. Res. Sect. A* **535**(1–2), 528–532 (2004).
11. R. Mirzoyan and E. Popova, “SiPM for atmospheric Cherenkov telescopes,” *Proc. SPIE* **8621**, 862106 (2013).
12. P. Buzhan et al., “The cross-talk problem in sipms and their use as light sensors for imaging atmospheric Cherenkov telescopes,” *Nucl. Instrum. Methods Phys. Res. Sect. A* **610**(1), 131–134 (2009).
13. G. Ambrosi et al., “Large size sipm matrix for imaging atmospheric Cherenkov telescopes applications,” *Nucl. Instrum. Methods Phys. Res. Sect. A* **824**, 125–127 (2016).
14. K. Yamamoto et al., “Recent development of mppc at hamamatsu for photon counting applications,” in *Proc. 5th Int. Workshop New Photon-Detectors*, p. 011001 (2019).
15. Hewlett Packard, “Low noise, cascadable silicon bipolar MMIC amplifier Technical Data,” <https://www.qsl.net/n9zia/metricom/ina02184.pdf> (accessed 17 May 2020).
16. Tektronix, “Mixed Signal Oscilloscopes MSO4000 Series, DPO4000 Series Data Sheet,” <https://download.tek.com/datasheet/MSO4000-DPO4000-Mixed-Signal-Oscilloscope-Datasheet-3GW2015624.pdf> (accessed 17 May 2020).
17. V. Álvarez et al., “Design and characterization of the SiPM tracking system of next-demo, a demonstrator prototype of the next-100 experiment,” *J. Instrum.* **8**(05), T05002 (2013).
18. E. Segreto et al., “Liquid argon test of the ARAPUCA device,” *J. Instrum.* **13**(08), P08021 (2018).
19. G. J. McLachlan and D. Peel, *Finite Mixture Models*, John Wiley & Sons (2004).
20. G. J. McLachlan and D. Peel, *Finite Mixture Models* John Wiley & Sons (2000).
21. D. Arthur and S. Vassilvitskii, “k-means++: the advantages of careful seeding,” in *Proc. Eighteenth Annu. ACM-SIAM Symp. Discrete Algorithms*, Society for Industrial and Applied Mathematics, pp. 1027–1035 (2007).
22. Gaia Collaboration et al., “Description of the Gaia mission (spacecraft, instruments, survey and measurement principles, and operations),” Gaia Collaboration et al.(2016a): Summary description of Gaia DR1 (2016).
23. A. G. A. Brown et al., “Gaia Data Release 2-Summary of the contents and survey properties,” *A & A* **616**, A1 (2018).
24. F. Kasten and A. T. Young, “Revised optical air mass tables and approximation formula,” *Appl. Opt.* **28**(22), 4735–4738 (1989).
25. A. Kinkhabwala and S. Thorsett, “Multifrequency observations of giant radio pulses from the millisecond pulsar B1937+ 21,” *Astrophys. J.* **535**(1), 365 (2000).
26. M. Shafee, S. Feghhi, and J. Rahighi, “Analysis of de-noising methods to improve the precision of the ILSF BPM electronic readout system,” *J. Instrum.* **11**(12), P12020 (2016).
27. M. Shafee, S. Feghhi, and J. Rahighi, “Experimental performance evaluation of ILSF BPM data acquisition system,” *Measurement* **100**, 205–212 (2017).
28. European Space Agency, “Gaia Science Community,” 2020, <https://www.cosmos.esa.int/gaia> (accessed 17 May 2020).
29. European Space Agency, “The DPAC Consortium,” 2020, <https://www.cosmos.esa.int/web/gaia/dpac/consortium> (accessed 17 May 2020).

**Albert W. K. Lau** is a PhD student in physics at Hong Kong University of Science and Technology, supervised by Professor George Smoot. He works mainly in developing photon detector system with high-temporal resolution for cosmological and astrophysical observation.

**Mehdi Shafee** is a post doc researcher at Queen’s University and former researcher at Nazarbayev University with a PhD in radiation application technologies. He worked on beam position monitoring systems for his PhD. His developed system could measure electron position inside of storage rings with 12- $\mu\text{m}$  resolution. He is skilled in superconducting detectors such as

microwave kinetic inductance detector, radiation detectors, astronomy, cosmology and accelerator instrumentation and data acquisition systems, expert in FPGAs, coding, and data processing.

**Siyang Li** is a PhD student in astronomy and astrophysics at Johns Hopkins University. He is currently a member of the Supernovae and H0 for the Equation of State (SH0ES) team and uses Hubble Space Telescope observations to reduce uncertainty in the cosmic distance ladder and Hubble constant. In 2020, he received his bachelor's degree in physics from the University of California, Berkeley, where he worked on developing the ultra-fast astronomy (UFA) silicon photomultiplier telescope.

**Zhanat Maksut** works as a research-engineer in the Energetic Cosmos Laboratory at Nazarbayev University. He has a master's degree in space science and technology from the Technical University of Munich. Currently, he is working on the automation process of the NUTTelA-TAO telescope in the Assy-Turgen Observatory, and observation of the prompt emission and early afterglow of GRBs in three optical bands.

Biographies of the other authors are not available.